Eur. Phys. J. A **8**, 187–196 (2000)

THE EUROPEAN PHYSICAL JOURNAL A

Description of long-range alpha emission using the sudden approximation

O. Serot[1,a], N. Carjan[2,b], and C. Wagemans[3,c]

[1] EC, JRC, Institute for Reference Materials and Measurements, Retieseweg, B-2440 Geel, Belgium
[2] CEN de Bordeaux-Gradignan, Le Haut Vigneau, F-33170 Gradignan, France
[3] Department of Subatomic and Radiation Physics, RUG, Proeftuinstraat 86, B-9000 Gent, Belgium

Received: 13 March 2000
Communicated by P. Schuck

Abstract. Long-Range Alpha (LRA) emission probability is studied using a one dimensional sudden approximation model. The probability of the energy transfer between the scissioning nucleus and the LRA particle as well as the LRA angular distribution are discussed for several elongations and for several mass splits at scission. Finally, it is shown that a comparison between the calculated LRA emission probability and the corresponding experimental data allows a determination of the Q_α-value at the scission point.

PACS. 21.60.Gx Cluster model – 23.60.+e α-decay – 24.75.+i General properties of fission – 25.85.Ca spontaneous fission

1 Introduction

Recent measurements of the characteristics of Long-Range Alpha (LRA) particles emitted during spontaneous fission of ^{238,240,242,244}Pu isotopes have enlightened the LRA emission process [1]. In particular, it has been shown that the LRA emission process occurs only if three conditions are fulfilled:

1) An α-cluster is formed inside the fissioning nucleus [2]. The α-preformation probability is calculated from the spectroscopic factor (S_α) determined in α-decay. It means that S_α is supposed to be rather constant during the fission process. This asumption is also supported by the calculations performed by Carjan *et al.* [3].
2) The available energy is larger than a minimum quantity that is related to the Energy Cost (E_c) (introduced by Halpern [4]) which corresponds to the energy needed to put an α-particle between the two fragments. Supposing that E_c is taken from the deformation energy of the scissioning nucleus, the probability (P_def) that this deformation energy is larger than E_c can be obtained from the distribution of the Total eXcitation Energy (TXE) in binary fission: P_def =Proba(TXE > E_c). Indeed, in the case of spontaneous fission, TXE is a good approximation of the deformation energy at scission, the internal heating being low [5].
3) At least this minimum energy E_c is effectively transfered to the α-particle. In this case, the α-particle can overcome the Coulomb barrier and escape from the nucleus. The calculation of the probability of this energy TRansfer between the scissioning nucleus and the LRA particle (P_TR) requires a mechanism by which this energy transfer occurs.

Moreover, it has also been shown in ref. [1] that the fission modes (the different paths taken by the fissioning nucleus from saddle to scission) have a strong impact both on the available energy (point 2) and on the energy that is effectively transferred (point 3). The impact of the fission modes on the available energy is reflected in the big difference between the corresponding TXE distributions. For instance, in the case of ^{238}Pu, the TXE distributions of the Standard I and Standard II fission modes (following Brosa's terminology [6]) are well described by Gaussians with an average value of 14.4 MeV (for St.I) and 24.2 MeV (for St.II) and with a full width at half maximum of 12.6 MeV (for St.I) and 23.5 MeV (for St.II). Moreover, P_TR was found to be much smaller in the (more compact) Standard I mode than in the (more elongated) Standard II mode. This means that P_TR increases with the deformation at scission.

Taking into account the three conditions mentioned above and including the effect of the fission modes, the LRA emission probability (given by the ratio of the LRA yield to the Binary fission yield: LRA/B) can be expressed by the following empirical formula:

$$LRA/B = S_\alpha \sum_i W^i \mathrm{Proba}^i(\mathrm{TXE} > E_\mathrm{c}^i) P_\mathrm{TR}^i \qquad (1)$$

[a] e-mail: serot@irmm.jrc.be
[b] e-mail: carjan@in2p3.fr
[c] e-mail: wagemans@irmm.jrc.be

where i indicates the fission mode and W^i its corresponding weight.

In eq. (1) the only quantity to be determined theoretically is $P_{\rm TR}$. For this purpose, we need a model for the mechanism by which the fissioning system transfers part of its available energy to the LRA particle. Such a model is realistic if it leads to the following predictions:

- the calculated $P_{\rm TR}$ values are strongly enhanced with the nuclear elongation at scission;
- the energy transfer is such that it explains the characteristics of the LRA angular distribution; in other words, this mechanism must lead to both equatorial and polar emission of LRA particles.

The aim of the present work is to show that the "sudden approximation" constitutes such a model. This emission mechanism was proposed long time ago by Halpern [4], but it has never been developed quantitatively. In this work, the sudden approximation is treated in one dimension, namely the deformation axis z. In the first part, we will present our model and the observables which can be calculated with it. In the second part, we will present and discuss our main results. Finally, we will show how an upper limit of the Q_α-value at the scission point ($Q_\alpha^{\rm SC}$) can be deduced from a comparison between our theoretical approach and the experimental data given in ref. [1]. This quantity is not accessible by any other means.

2 Description of the model

The idea of the sudden approximation is the following: an α-particle is in a potential that changes so rapidly during the neck rupture that the particle has no time to "follow" this change. The potential change is due to the sudden rupture of the neck between the nascent fission fragments and its absorption by the fragments. Since in this case, the α-motion is not at all adiabatic, the α-particle can be described "Immediately After Scission" (IAS) by the same wave function as "Just Before Scission" (JBS). The sudden approximation is only justified if the typical neck rupture time is very small compared to the typical period of motion for an α-particle inside the scissionning nucleus.

2.1 Parametrisation of the shape and calculation of the potential

The quantitative results were obtained under the assumption that the IAS shape is described by two spherical fragments with the same distance between the center of mass ($D_{\rm cm}$) and the same mass asymmetry ($R = M_H/M_L$) as the JBS shape. To describe the nuclear shape at JBS time, we have used the parametrisation of Brack *et al.* [7]:

$$\rho^2_{\rm JBS}(z) = \left(d^2 - z^2\right)\left(A + \alpha\left(\frac{z}{d}\right) + B\left(\frac{z^2}{d^2}\right)\right), \qquad (2)$$

where $\rho_{\rm JBS}$ and z are the cylindrical coordinates of the nucleus and A, B, α and d are four parameters. Due to the volume conservation constraint, only three of them are free. These free parameters control three characteristics of the JBS shape:

- the distance between the two centers of mass of the nascent fragments: $D_{\rm cm}$;
- the mass asymmetry of the fragments: $R = M_H/M_L$;
- the diameter of the neck: $d_{\rm neck}$.

For the IAS nuclear shape, the formula (2) is no longer used since we suppose two spherical fragments (keeping the same $D_{\rm cm}$ and R as the JBS nuclear shape). Examples of JBS and IAS shapes are shown in fig. 1 for two sets of parameters: $R = 1$, $D_{\rm cm}$=18.2 fm and $d_{\rm neck}$=2.4 fm (left side) and $R = 1.4$, $D_{\rm cm}$=20.5 fm and $d_{\rm neck}$=2.4 fm (right side).

The potential along the z-axis (potential in one dimension) is calculated by summing the nuclear ($V_{\rm nuc}$) and coulomb ($V_{\rm coul}$) part seen by an α-particle. The nuclear interaction is given by a deformed Woods-Saxon type of potential. The depth ($V_0 = -96.4$ MeV), the diffuseness ($a = 0.625$ fm) and the range ($r_0 A^{1/3}$ with $r_0 = 1.376$ fm) of this potential are chosen in order to reproduce α-scattering data [8]. The coulomb part is obtained supposing a uniform charge density inside the surface defined by eq. (2). All the details of the calculation can be found in ref. [9], where the authors have considered the same potential in their quantum-mechanical treatment of LRA emission.

2.2 Determination of $\psi^{\rm out}_{\rm LRA}$

In analogy with alpha-decay, the LRA wave function at the JBS time was supposed to be an eigenstate of the JBS potential:

$$|\,\psi_{\rm LRA}\rangle = |\,\varphi_n^{\rm JBS}\rangle, \qquad (3)$$

having an eigenenergy equal to the Q_α-value at scission: $E_n^{\rm JBS} = Q_\alpha^{\rm SC}$.

Due to the total loss of adiabaticity during the neck rupture, $\psi_{\rm LRA}$ is described at the IAS time by the same wave function (which is now a wave packet in the new IAS potential). In this way, $\psi_{\rm LRA}$ receives "suddenly" an amount of energy. This energy transfer mechanism allows the α-particle to have components with energy higher than the top of the potential barrier. Therefore, the part of the wave function with such components ($\psi^{\rm out}_{\rm LRA}$) corresponds to an α-particle able to escape from the nucleus. This can be seen using the following decomposition:

$$\begin{aligned}|\psi_{\rm LRA}\rangle = |\varphi_n^{\rm JBS}\rangle &= \sum_m \langle\varphi_m^{\rm IAS}|\psi_{\rm LRA}\rangle|\varphi_m^{\rm IAS}\rangle \\ &\quad + \int_E \langle\varphi_E^{\rm IAS}|\psi_{\rm LRA}\rangle|\varphi_E^{\rm IAS}\rangle {\rm d}E \\ &= |\psi^{\rm in}_{\rm LRA}\rangle + |\psi^{\rm out}_{\rm LRA}\rangle\end{aligned}$$

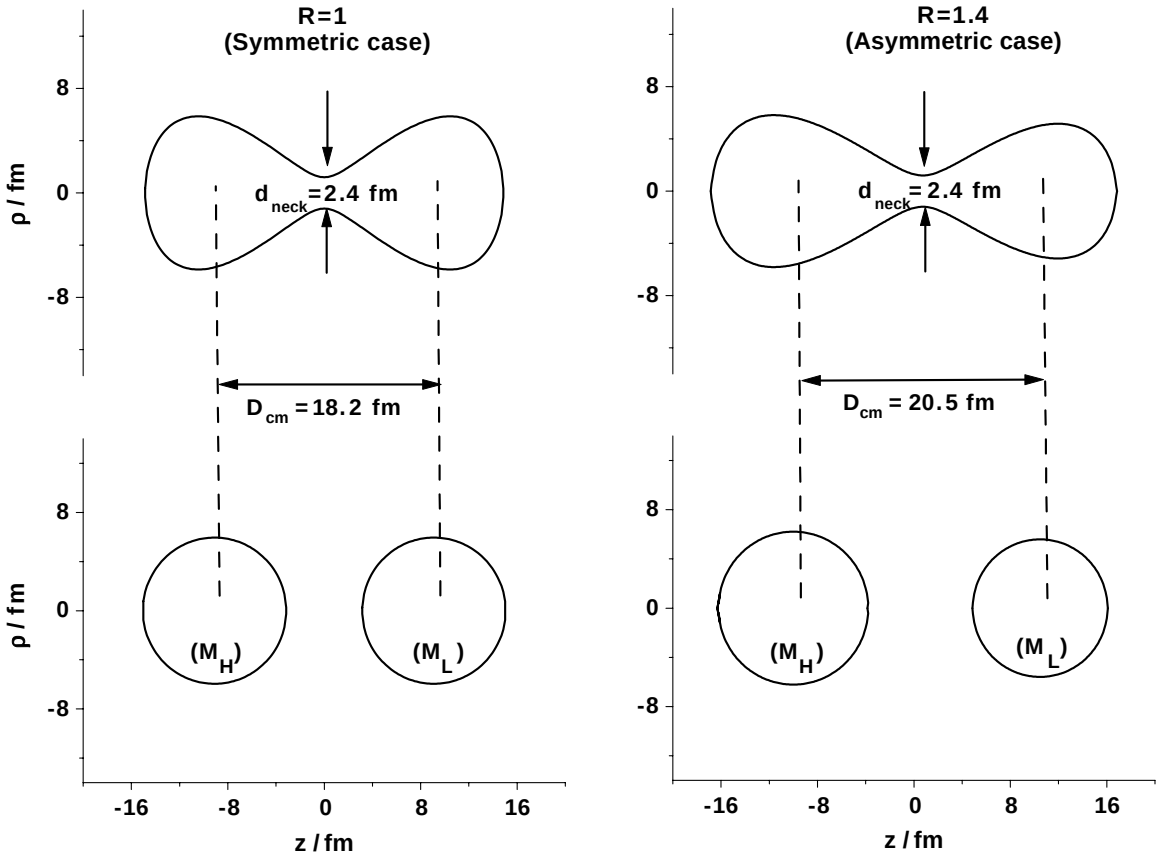

Fig. 1. Examples of "Just Before Scission" (top) and "Immediately After Scission" (bottom) nuclear shapes obtained for $A = 240$ with two different sets of parameters: $D_{\rm cm}$=18.2 fm, $R = 1$, $d_{\rm neck}$=2.4 fm (left) and $D_{\rm cm}$=20.5 fm, $R = 1.4$, $d_{\rm neck}$=2.4 fm (right).

where $\{|\ \varphi_m^{\rm IAS}\rangle\}$ and $\{|\ \varphi_E^{\rm IAS}\rangle\}$ are the eigenstates of the IAS potential, respectively, below and above the top of the barrier. The term $|\psi_{\rm LRA}^{\rm in}\rangle = \sum_m \langle\varphi_m^{\rm IAS}|\psi_{\rm LRA}\rangle|\varphi_m^{\rm IAS}\rangle$ corresponds to the LRA-wave function having components lower than the top of the IAS potential barrier, while the term $|\psi_{\rm LRA}^{\rm out}\rangle = \int_E \langle\varphi_E^{\rm IAS}|\psi_{\rm LRA}\rangle|\varphi_E^{\rm IAS}\rangle {\rm d}E$ represents the LRA-wave function with components higher than the top of the IAS potential barrier. Consequently, $\psi_{\rm LRA}^{\rm in}$ describes the α-particles staying inside the nascent fragments while $\psi_{\rm LRA}^{\rm out}$ describes the α-particles escaping from the nucleus. Since the diagonalisation of the potential cannot give us the eigenstates of the continuum, $\psi_{\rm LRA}^{\rm out}$ cannot be obtained directly but from the difference between $\psi_{\rm LRA}$ and $\psi_{\rm LRA}^{\rm in}$:

$$|\psi_{\rm LRA}^{\rm out}\rangle = |\varphi_n^{\rm JBS}\rangle - \sum_m \langle\varphi_m^{\rm IAS}|\varphi_n^{\rm JBS}\rangle|\varphi_m^{\rm IAS}\rangle. \qquad (4)$$

2.3 Deduced observables

The knowledge of $\psi_{\rm LRA}^{\rm out}$ allows the determination of two physical quantities:

– the probability $P_{\rm TR}$ to transfer enough energy to emit an α-particle which is simply given by

$$P_{\rm TR} = \int_{-\infty}^{+\infty} |\ \psi_{\rm LRA}^{\rm out}(z)\ |^2\ {\rm d}z \qquad (5)$$

– the LRA angular distribution. Indeed, since $|\psi_{\rm LRA}^{\rm out}(z)|^2$ represents the probability of the released α-particles to be present outside the nucleus (*e.g.* at the ridge of the α-nucleus potential), $|\ \psi_{\rm LRA}^{\rm out}(z)\ |^2$ is related to the LRA angular distribution. Nevertheless, we need to know the correspondance between the initial position $(\rho_{\rm ridge}, z)$ of an LRA-particle and its final angle $\theta_{\alpha L}$ with respect to the light fragment. This correspondance is given by the deflection function $\theta_{\alpha L}(z)$, which can be obtained from classical trajectory calculations of an α-particle moving in the field of the two main fragments. Such classical calculations have been already performed by Carjan and Leroux [10] where the finite size of the fragments was taken into account. Then, knowing $\theta_{\alpha L}(z)$ (from [10] and [11]) and $|\psi_{\rm LRA}^{\rm out}(z)|^2$ (from the present work), the theoretical LRA angular distribution can be deduced from the

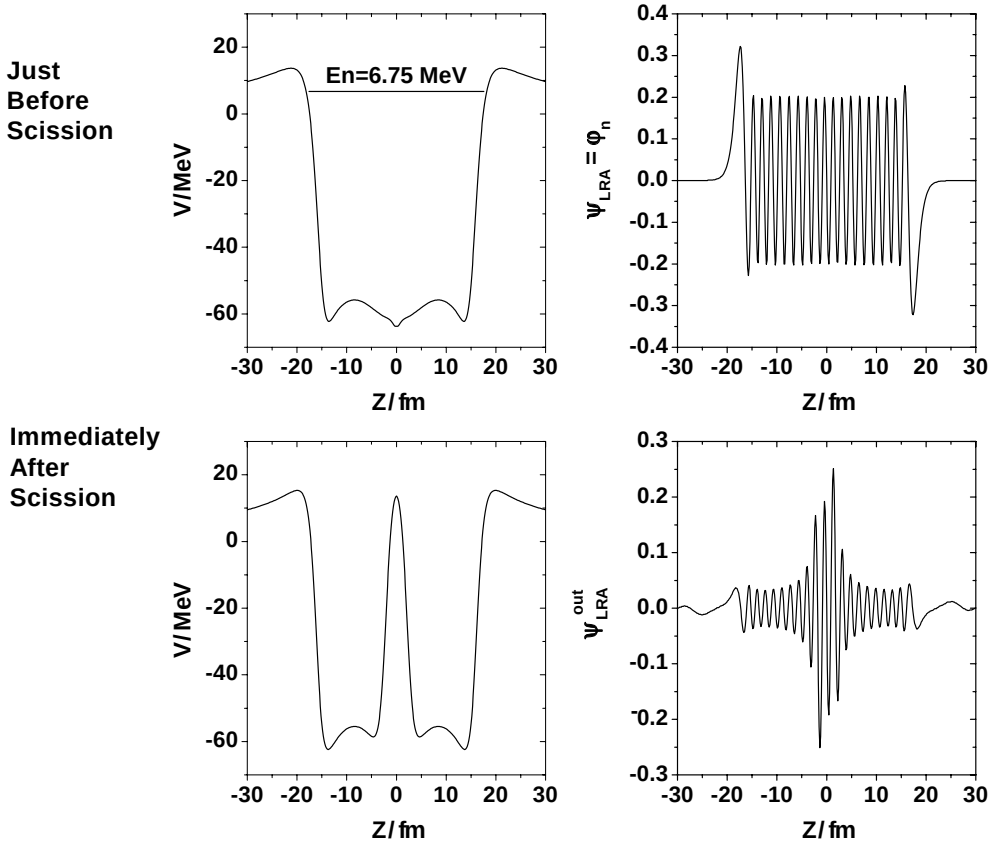

Fig. 2. Typical example of the procedure used to determine $\psi^{\rm out}_{\rm LRA}$. The plots on the top of the figure represent the potential (left) and the wave function (right) at the "Just Before Scission" time. The situation after the sudden neck rupture (corresponding to the "Immediatly after scission" time) is illustrated on the bottom of the figure, where the potential (left) and $\psi^{\rm out}_{\rm LRA}$ deduced from eq. (4) (right) are plotted. The parameters used in this example are: $D_{\rm cm} = 18.2$ fm, $R = 1$ (symmetric case), $d_{\rm neck} = 2.4$ fm and $Q^{\rm SC}_{\alpha} = 6.75$ MeV.

following equation [11]:

$$N_{\rm th}(\theta_{\alpha L}) = \sum_{Z} |\psi^{\rm out}_{\rm LRA}(z)|^2 \rho_{\rm ridge}(z) \sqrt{1 + \left(\frac{{\rm d}\rho_{\rm ridge}}{{\rm d}z}\right)^2} \left|\frac{{\rm d}\theta_{\alpha L}}{{\rm d}z}\right|^{-1}, \quad (6)$$

where $\rho_{\rm ridge}(z)$ defines the line on which the LRA are located when the classical trajectory calculations start: this line corresponds to the ridge of the potential barrier and is situated at about 2 fm from the nuclear surface. The sum is done over all the z-positions leading to the same final angle $\theta_{\alpha L}$. Moreover, in order to simulate a finite experimental angular resolution, we have to make a convolution of $N_{\rm th}(\theta_{\alpha L})$ with an angular resolution function $r(\theta)$ (which is supposed to be a Gaussian function). In this way, eq. (6) becomes

$$N_{\rm exp}(\theta_{\alpha L}) = \frac{A}{\omega\sqrt{2\pi}} \int_{-\infty}^{+\infty} N_{\rm th}(\theta) \exp\left(-\frac{(\theta_{\alpha L} - \theta)^2}{2\omega^2}\right) {\rm d}\theta, \quad (7)$$

where A is a normalisation constant and ω the experimental angular resolution. We have taken here: $\omega = 2^\circ$.

From eq. (7), the equatorial (between fragments) and polar (beyond fragments) contributions of the LRA angular distribution can be separated.

2.4 Typical example

A typical example of numerical results obtained for ^{240}Pu using the procedure described above is shown in figs. 2 and 3.

Figure 2 illustrates the several steps used for the determination of $\psi^{\rm out}_{\rm LRA}$. In this example, the parameters used to get the nuclear shapes are: $D_{\rm cm} = 18.2$ fm, $R = 1$ (symmetric case) and $d_{\rm neck} = 2.4$ fm. The JBS and IAS potentials can be seen in the left-top and left-bottom of the figure, respectively. Knowing the JBS potential, we have calculated the corresponding eigenstates. Then, we have chosen one of these eigenstates as the initial wave function. Here, the 37th eigenstate ($\psi_{\rm LRA} = \varphi^{\rm JBS}_{37}$) with $E^{\rm JBS}_{37} = Q^{\rm SC}_{\alpha} = 6.75$ MeV was considered and plotted on the right-top of fig. 2. From the calculations of the eigenstates of the IAS potential, eq. (4) can be applied in order to get $\psi^{\rm out}_{\rm LRA}$ which is plotted on the right-bottom of fig. 2. From eq. (5), we have obtained: $P_{\rm TR}$=0.16. The eigenstates of both JBS

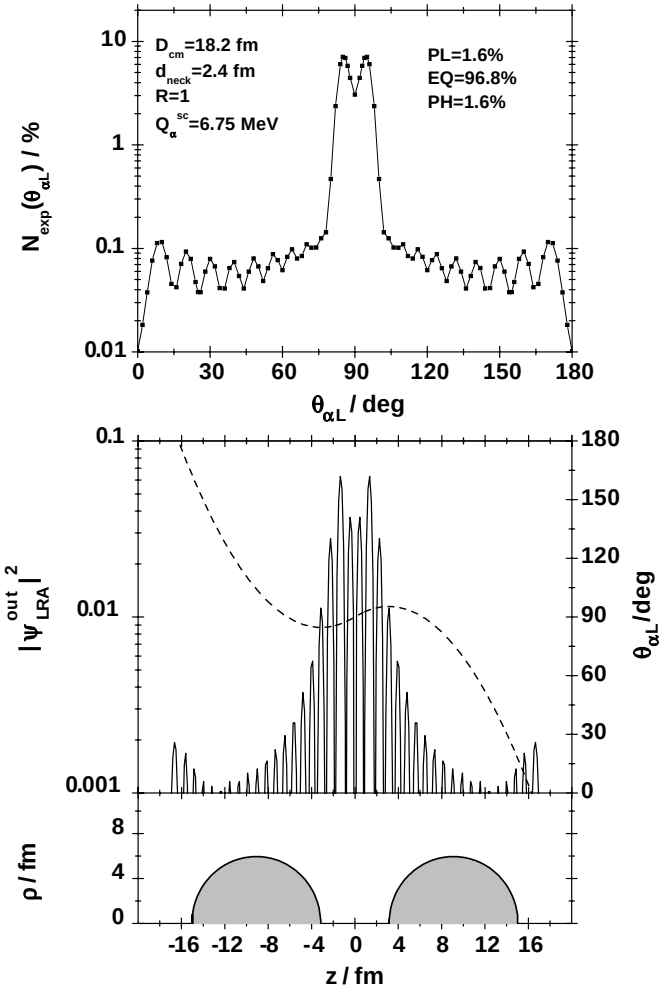

Fig. 3. LRA angular distribution (top of the figure) obtained from eq. (7) using the same parameters as in fig. 2. The IAS shape is plotted on the bottom part while $\mid \psi_{\rm LRA}^{\rm out} \mid^2$ (straight line, left-hand-logarythmic scale) and $\theta_{\alpha L}$ (dashed line, right-hand scale) are drawn in the middle part. Note that the Polar Light (PL), Polar Heavy (PH) and EQuatorial (EQ) contributions of the LRA angular distribution are also mentioned.

and IAS potentials were obtained by solving numerically the corresponding stationary Schrödinger equation on the following grid: $z = -40$ fm to $z = +40$ fm by $\Delta z = 0.15$ fm.

Figure 3 is related to the LRA angular distribution which was deduced from $\psi_{\rm LRA}^{\rm out}$. On the bottom of the figure, the IAS shape is again drawn. $|\psi_{\rm LRA}^{\rm out}|^2$ is plotted in the middle part (straight line and left-hand logarythmic scale). We can already observe that the main part of $|\psi_{\rm LRA}^{\rm out}|^2$ is located between the heavy fragments and it is due to the strong potential change in the neck region between JBS time and IAS time. This main part will contribute to the equatorial emission. The much smaller variation of the potential at the extremities of the fragments produces small contributions of $|\psi_{\rm LRA}^{\rm out}|^2$ in this region. This part will correspond to the polar emission. The deflection function $\theta_{\alpha L}(z)$ taken from ref. [11], is also plotted in the middle of fig. 3 (dashed line and right-hand scale). Finally, the LRA angular distribution calculated using eq. (7) can be seen on the top part of fig. 3. From these distribution, the polar emission ($\theta_{\alpha L} \in [0°, 25°]$ and $\theta_{\alpha L} \in [155°, 180°]$) as well as the equatorial emission $\theta_{\alpha L} \in [25°, 155°]$ can be deduced: we have obtained, respectively, 1.6% and 96.8%.

3 Results and discussion

As we have seen, our model contains four free parameters: three of them ($D_{\rm cm}$, $d_{\rm neck}$ and R) come from the JBS shape while the fourth one ($Q_\alpha^{\rm SC}$) comes from the choice of the initial LRA wave function (*i.e.* from the JBS eigenstate). The influence of these parameters on $\psi_{\rm LRA}^{\rm out}$ will now be studied and discussed. In fact, we already noticed that $\psi_{\rm LRA}^{\rm out}$ is strongly influenced by the difference between the JBS and IAS potentials. In our one-dimensional calculations, for a given $D_{\rm cm}$ and R value, the variation of the $d_{\rm neck}$ has a negligible effect on the JBS potential along the z-axis (and of course, no effect on the IAS potential). Therefore, the $d_{\rm neck}$ parameter has a negligible influence on the calculated $\psi_{\rm LRA}^{\rm out}$. This is the reason why we have adopted a fixed $d_{\rm neck}$ value of 2.4 fm for all calculations.

3.1 Angular distribution

To study the influence of the mass asymmetry (R) and of the elongation ($D_{\rm cm}$) on the LRA angular distribution, three cases have been considered:

- $D_{\rm cm} = 18.2$ fm and $R = 1$ (case a);
- $D_{\rm cm} = 20.5$ fm and $R = 1$ (case b) and
- $D_{\rm cm} = 20.5$ fm and $R = 1.4$ (case c).

For each case, the choice of the initial LRA wave function (eq. (3)) was done in such a way that they all have the $Q_\alpha^{\rm SC}$ value of 2 MeV. For each R and $D_{\rm cm}$ values, the corresponding deflection function was taken from [11]. These three cases are illustrated in fig. 4, using the same presentation as in fig. 3 (except for $\mid \psi_{\rm LRA}^{\rm out} \mid^2$ which is plotted on a linear scale).

It is interesting to observe that in all cases, $N_{\rm exp}(\theta_{\alpha L})$ (top of fig. 4), corresponding to an angular resolution of 2°, has two close peaks in the equatorial region. These peaks correspond to the two extrema of the deflection function. It has been shown [11] that this structure could be experimentally observed only with an experimental angular resolution lower than 5° and with a narrow selection on the fragment masses.

Comparing cases a and b (same mass asymmetry but different elongation), we can observe that the elongation of the scissioning nucleus has two main effects, namely an increase of the polar contribution and of the width of the equatorial contribution. This is in qualitative agreement with the experimental data obtained by Heeg [12] (for ^{252}Cf(sf)) and Theobald *et al.* [13] (for ^{235}U(n,f)). Indeed, these authors have analysed the LRA angular distribution for different mass splits. They have shown that for

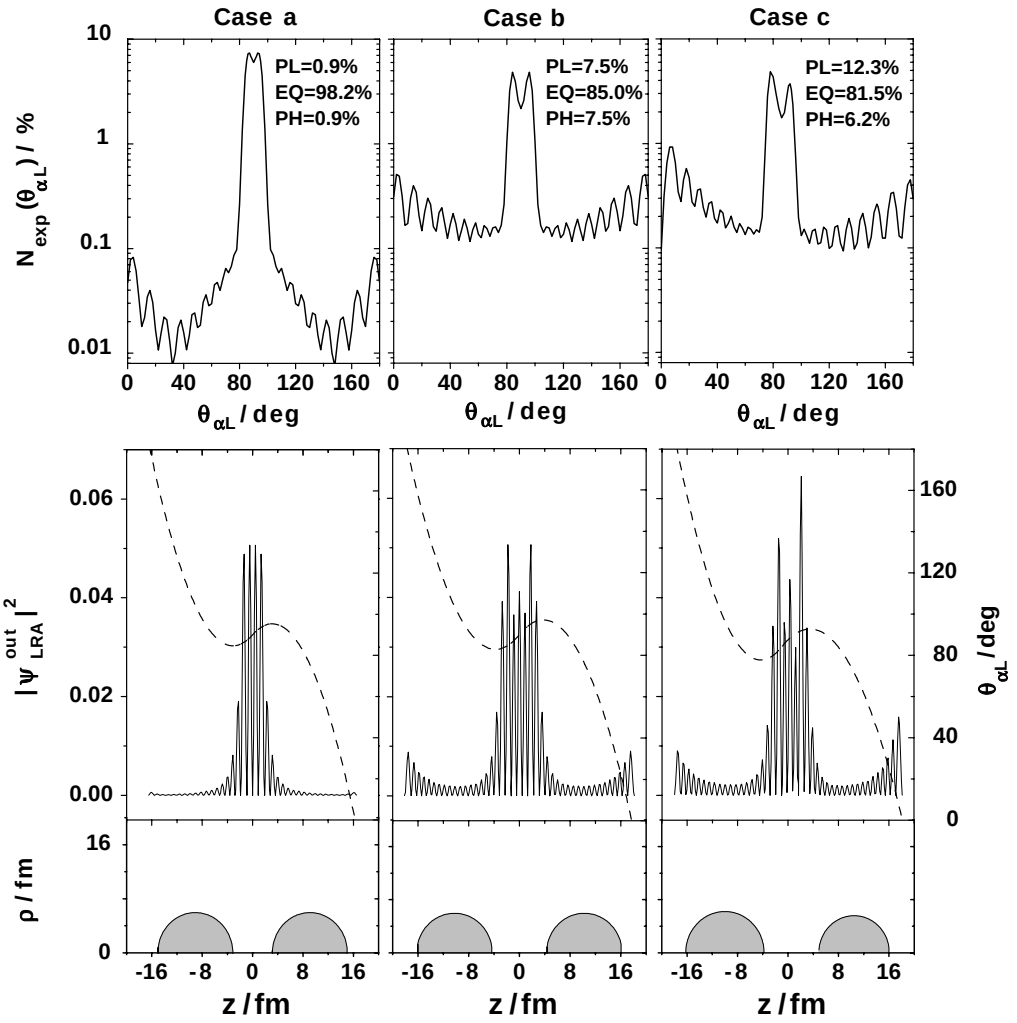

Fig. 4. The same as in fig. 3 but for the three following cases: $D_{\rm cm} = 18.2$ fm, $R = 1$ (case a on the left part); $D_{\rm cm} = 20.5$ fm, $R = 1$ (case b in the middle) and $D_{\rm cm} = 20.5$ fm, $R = 1.4$ (case c on the right part). In all cases, the JBS wave function was chosen in order to have $Q_\alpha^{\rm SC} \sim 2$ MeV. Note that the Polar Light (PL), Polar Heavy (PH) and EQuatorial (EQ) contributions of the LRA angular distribution are also mentioned.

the symmetric case ($1.0 < R < 1.2$), which corresponds to the so-called Super Long fission mode [6] (*i.e* to the more elongated scissioning configuration), the width of the angular distribution as well as the polar contribution are enhanced compared to other R values.

Comparing cases b and c (same elongation but different mass split), we can observe that the main difference is the increase of the polar light contribution ($\theta_{\alpha L} \in [0°, 25°]$) when the mass asymmetry is increasing. For instance, in case b ($R = 1$), both polar contributions represent 7.5% of the total angular distribution, while in case c ($R = 1.4$), the heavy polar contribution slighlty decreases (6.2%) and the light polar one reaches 12.3%. This enhancement of the light polar emission with mass asymmetry is also observed experimentally [12].

Hence, the sudden approximation allows us to understand and to reproduce qualitatively the main characteristics of the LRA angular distribution. Quantitatively however, the polar contributions as well as the width of the equatorial distribution are too high. This is a consequence of our two spherical fragments approximation of the IAS configuration. Indeed, with a more realistic fragment shape, the change between the JBS and IAS potentials at the extremities of the fragments as well as in the neck region would be less pronounced and consequently both the polar emission and the width of the equatorial emission would be reduced.

3.2 Energy transfer probability $P_{\rm TR}$

Concerning the energy transfer probability, we can observe the following properties:

– the influence of the mass asymmetry on $P_{\rm TR}$ is negligible. Indeed, the R parameter will affect the repartition of the polar and equatorial contributions but the integral value will stay quite constant.

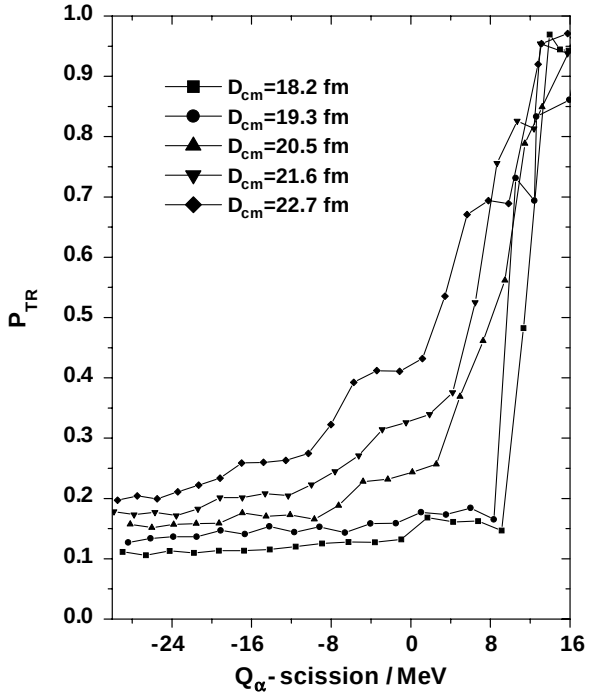

Fig. 5. Energy transfer probability ($P_{\rm TR}$) as a function of the Q_α-scission value for five different elongations at scission.

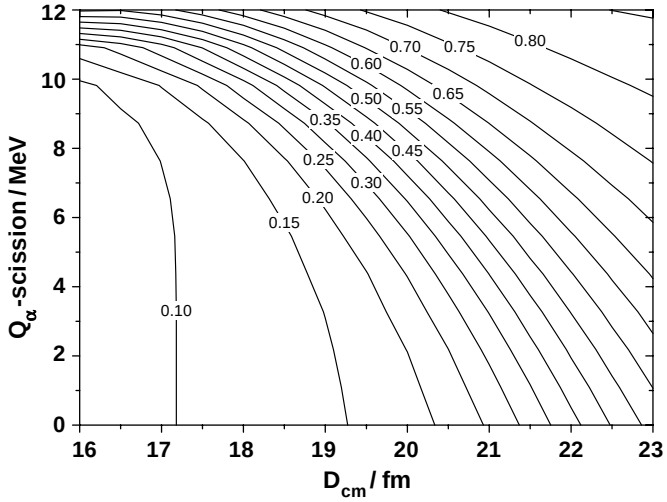

Fig. 6. Two-dimensional plot of $P_{\rm TR}$ as a function of $D_{\rm cm}$ and $Q_\alpha^{\rm SC}$ obtained from the procedure described in appendix B.

– $P_{\rm TR}$ depends on the distance between the center-of-mass of the fragments as well as on the Q_α-scission value: $P_{\rm TR} \equiv P_{\rm TR}(D_{\rm cm}, Q_\alpha^{\rm SC})$. This is shown in fig. 5 where $P_{\rm TR}$ has been calculated for all the eigenfunctions $\varphi_n^{\rm JBS}$ below the top of the barrier and for several elongations. Fitting our calculation and extrapolating for intermediate $D_{\rm cm}$ values (see appendix B for the details of this fitting procedure) we have obtained a contour plot of $P_{\rm TR}$ (fig. 6).

For a given Q_α-scission value, we can see that $P_{\rm TR}$ strongly increases with the elongation of the scissioning nucleus which is in agreement with the experimental data [1]. This property was also contained in the model of Carjan [2] as well as in its quantum-mechanical versions [9,14], but could not be reproduced in Rubchenya's model [15,16].

4 Determination of the Q_α-value at scission

4.1 Some comments on equation (1)

As mentioned in the introduction, the behaviour of the LRA emission probabilities for the Pu-isotopes [1] can be very well described using eq. (1). This equation can be derived in the following way.

For a fission event corresponding to a given available energy TXE, the LRA emission probability can be written as

$$(LRA/B)_{\rm TXE} = S_\alpha W_{\rm TXE} \delta({\rm TXE} > E_{\rm c}) P_{\rm TR} \qquad (8)$$

$$\text{with } \begin{cases} \delta({\rm TXE} > E_{\rm c}) = 1 & \text{if} \quad {\rm TXE} > E_{\rm c}, \\ \delta({\rm TXE} > E_{\rm c}) = 0 & \text{otherwise}, \end{cases}$$

where $W_{\rm TXE}$ represents the statistical weight of the given TXE value. Equation (8) reflects the fact that when the available energy is too small (TXE $< E_{\rm c}$), LRA emission is not possible, while in the opposite case (TXE $> E_{\rm c}$), the energy transfer between the scissioning nucleus and the α-particle can occur with a finite probability $P_{\rm TR}$.

Considering all the fission events and keeping in mind that TXE is essentially depending on the mass asymmetry (R) and on the scission elongation ($D_{\rm cm}$), eq. (8) can be generalised:

$$LRA/B = S_\alpha \sum_{i=I,II} W^i \times \iint {\rm d}R^i {\rm d}D^i_{\rm cm} W_{\rm TXE} \delta({\rm TXE} > E^i_{\rm c}) P^i_{\rm TR}(D^i_{\rm cm}, Q^{\rm SC}_\alpha), \qquad (9)$$

since $P^i_{\rm TR}$ is not affected by the mass asymmetry (see last paragraph). On the other hand, according to Brosa's theory, for a given fission mode i, the distribution of the scission elongations is strongly peaked on the average scission elongation $\langle D^i_{\rm cm} \rangle$ and therefore $P^i_{\rm TR}$ does not depend on TXE. So, we can reasonably make the following approximation:

$$P^i_{\rm TR}\left(D^i_{\rm cm}, R^i, Q^{\rm SC}_\alpha\right) \simeq P^i_{\rm TR}\left(\langle D^i_{\rm cm}\rangle, Q^{\rm SC}_\alpha\right). \qquad (10)$$

Using approximation (10), $P^i_{\rm TR}$ can be put outside the double integral in eq. (9). Moreover, since $\iint {\rm d}R^i {\rm d}D^i_{\rm cm}$ $W_{\rm TXE}\delta({\rm TXE} > E^i_{\rm c})$ =Proba(TXE $> E^i_{\rm c}$), we can see that eq. (1) is simply resulting from eqs. (9) and (10).

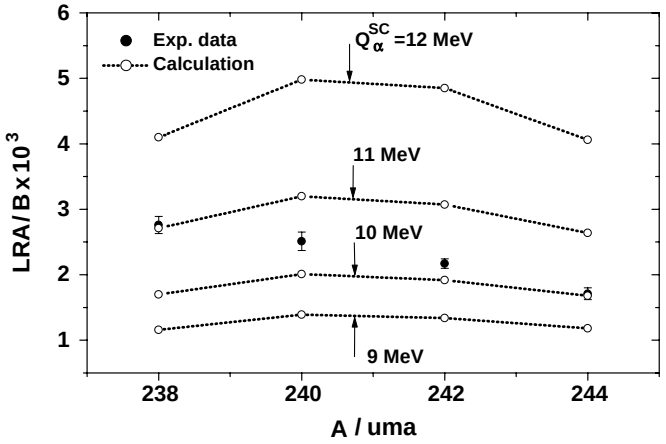

Fig. 7. Experimental (solid circle) and calculated (open circle) LRA/B-values for the four Pu-isotopes under investigation (^{238,240,242,244}Pu). The $Q_\alpha^{\rm SC}$ values used for the calculations are also mentioned. It can be seen that the best agreement is reached when $Q_\alpha^{\rm SC}$ is between 10 and 11 MeV.

Table 1. Survey of the quantities needed to apply eq. (11). Except for S_α, all these data are extracted from the experimental work of ref. [17].

	S_α	Standard I		Standard II	
	(10^{-3})	$\langle D_{\rm cm}^{\rm I}\rangle$ (fm)	$W^{\rm I}$ Proba (%)	$\langle D_{\rm cm}^{\rm II}\rangle$ (fm)	$W^{\rm II}$Proba (%)
^{238}Pu	8.63	16.4	2.44	17.9	75.12
^{240}Pu	10.91	16.6	14.85	17.9	60.86
^{242}Pu	11.01	16.7	20.97	18.0	52.75
^{244}Pu	8.7	17.0	30.62	18.2	46.70

Table 2. Energy transfer probabilities ($P_{\rm TR}^i$ for i=St.I, St.II) and $Q_\alpha^{\rm SC}$-values deduced from a comparison between the experimental LRA/B data and our calculations. The $Q_\alpha^{\rm GS}$ values are also mentioned to show that the difference (ΔQ_α) between $Q_\alpha^{\rm SC}$ and $Q_\alpha^{\rm GS}$ stays rather constant for all Pu-isotopes. Note that it is also the case for the ratio $P_{\rm TR}^{\rm II}/P_{\rm TR}^{\rm I}$.

	$Q_\alpha^{\rm GS}$ (MeV)	$Q_\alpha^{\rm SC}$ (MeV)	$\Delta\, Q_\alpha$ (MeV)	$P_{\rm TR}^{\rm I}$	$P_{\rm TR}^{\rm II}$	$P_{\rm TR}^{\rm II}/P_{\rm TR}^{\rm I}$
^{238}Pu	5.6	11.0	5.4	0.22	0.42	1.9
^{240}Pu	5.3	10.5	5.2	0.16	0.34	2.1
^{242}Pu	5.0	10.3	5.3	0.15	0.32	2.1
^{244}Pu	4.7	10.0	5.3	0.16	0.32	2.0

4.2 Comparison with the experimental data

From a comparison between the experimental LRA emission probabilities and the theoretical LRA/B values obtained from eq. (1), we can extract a very useful physical quantity: $Q_\alpha^{\rm SC}$. Nevertheless, in order to apply eq. (1), we have to know the following quantities: S_α, W^i, the TXE distributions for each fission mode, $\langle D_{\rm cm}^i\rangle$ and $E_{\rm c}^i$. As mentioned in the introduction, S_α is determined from α-decay (see appendix A). W^i and the TXE distributions are known for each fission mode of all Pu-isotopes from the experimental work done by Demattè *et al.* [17]. The $\langle D_{\rm cm}^i\rangle$ values can be evaluated from the average total kinetic energy of the fragments in each fission mode. All these quantities are reported in table 1. Finally, in the frame of our sudden approximation, $E_{\rm c}^i$ is defined by the top of the IAS barrier: $E_{\rm c}^i = V_{\rm max}^i$. In fact, since the average scission elongations of the two fission modes are not very far apart, $V_{\rm max}^{\rm I}$ and $V_{\rm max}^{\rm II}$ are close: $V_{\rm max}^{\rm I} \simeq V_{\rm max}^{\rm II} \simeq 16$ MeV.

So, the LRA emission probability can be calculated for several Q_α-scission values using:

$$LRA/B = S_\alpha \times \Big\{ W^{\rm I}{\rm Proba}^{\rm I}\left({\rm TXE} > V_{\rm max}^{\rm I}\right) P_{\rm TR}^{\rm I}\left(\langle D_{\rm cm}^{\rm I}\rangle, Q_\alpha^{\rm SC}\right) + W^{\rm II}{\rm Proba}^{\rm II}\left({\rm TXE} > V_{\rm max}^{\rm II}\right) P_{\rm TR}^{\rm II}\left(\langle D_{\rm cm}^{\rm II}\rangle, Q_\alpha^{\rm SC}\right) \Big\}. \quad (11)$$

A comparison between the experimental and the theoretical LRA emission probabilities is shown in fig. 7. The best agreement is reached when $Q_\alpha^{\rm SC}$ is between 10 and 11 MeV. The $Q_\alpha^{\rm SC}$ values which exactly reproduce the experimental data are given in table 2 as well as the Q_α-Ground State values ($Q_\alpha^{\rm GS}$). Note that within the uncertainties, the differences ΔQ_α between $Q_\alpha^{\rm SC}$ and $Q_\alpha^{\rm GS}$ are approximatively the same for all Pu-isotopes, which gives confidence to our model. Furthermore, these relative values are in good agreement with the values obtained by Lestone *et al.* [18]. Nevertheless, the sudden approximation gives only an upper limit for the transfer probability since the transfer depends on the finite velocity of the change of the potential. This has consequences on the extracted $Q_\alpha^{\rm SC}$ values, which have therefore to be considered as upper limits.

Lastly, concerning the values of $P_{\rm TR}^{\rm I}$ and $P_{\rm TR}^{\rm II}$ (see table 2), we can again notice that the ratio $P_{\rm TR}^{\rm II}/P_{\rm TR}^{\rm I}$ stays rather constant for all nuclei.

5 Conclusions

The one-dimensional sudden approximation model presented in this article enables to describe the following aspects of LRA emission:

- The LRA angular distribution can be well explained and the main characteristics of the equatorial and polar contributions can be qualitatively reproduced. Nevertheless, more realistic fragment shapes must be considered in order to reproduce quantitatively the LRA angular distribution.
- The energy transfer probability is depending on the elongation of the scissioning nucleus. This is in agreement with the experimental evidence of the enhancement of $P_{\rm TR}$ in the more elongated Standard II fission mode than in the (more compact) Standard I fission mode.
- The LRA emission probability can be calculated and compared with experimental data; from this comparison an upper limit for the Q_α-scission value can be obtained.

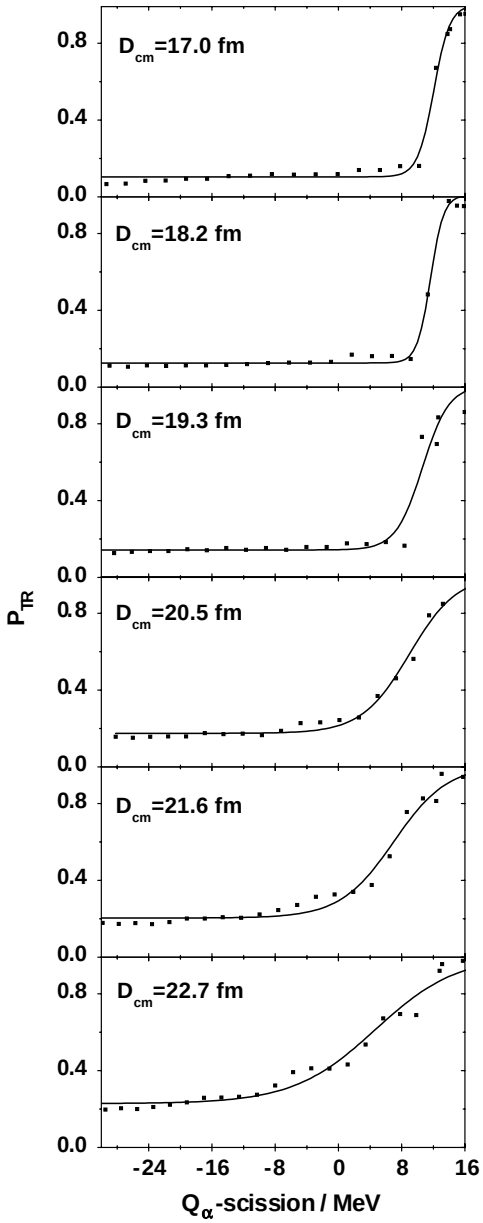

Fig. 8. Fit of the energy transfer probability as a function of the Q_α-scission value for six different elongations at scission. Both the calculated values (solid squares) and the fit curves (lines) are shown.

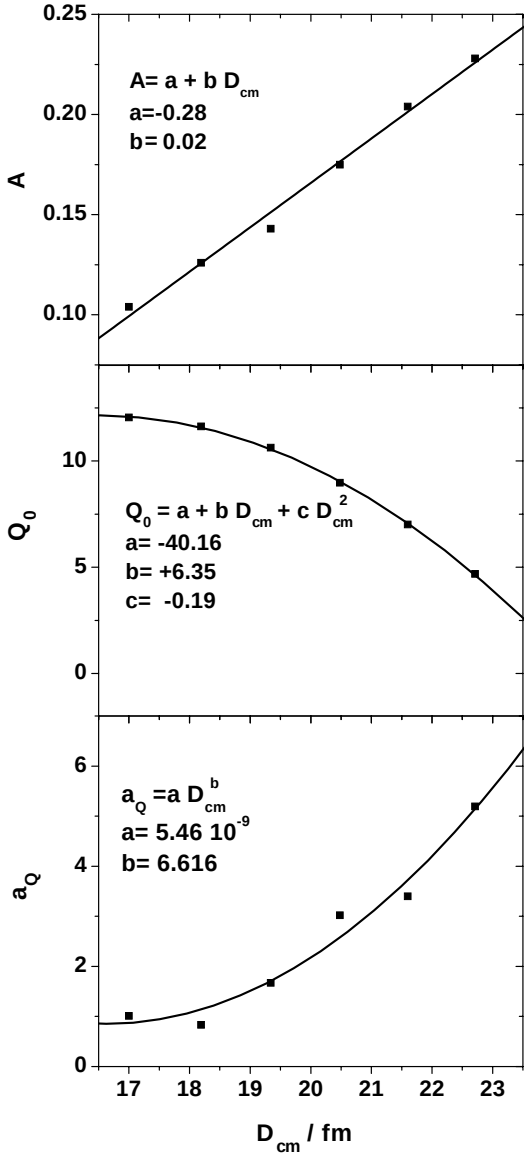

Fig. 9. Plot of the parameters A, Q_0 and a_Q as a function of $D_{\rm cm}$. The lines represent the best fits we have obtained. The fit functions are also written.

It is difficult to estimate the error introduced by the one-dimensional approximation. Therefore, the extension of this model to two dimensions should be a priority for future studies of LRA emission using the sudden approximation.

The authors thank Dr H. Weigmann for a careful reading of the manuscript.

Appendix A.

The spectroscopic factor S_α was calculated using the following formula:

$$S_\alpha = \frac{b\lambda_{\rm exp}}{\lambda_{\rm WKB}},$$

where b is the branching ratio for the ground state to ground-state transition; $\lambda_{\rm exp}$ the experimental α-decay constant and $\lambda_{\rm WKB}$ the α-decay constant calculated from the WKB approximation. The parameters used for the WKB approximation are the same as those described in sect. 2. The experimental values for b and $\lambda_{\rm exp}$ were taken from ref. [19]. The results of S_α obtained in this way are given table 1 for several Pu-isotopes.

Appendix B.

In order to deduce the two-dimensional plot of $P_{\rm TR}$ as a function of $D_{\rm cm}$ and $Q_\alpha^{\rm SC}$ (see fig. 6), we have used the following procedure:

- First, we have calculated $P_{\rm TR}$ for six different $D_{\rm cm}$ values: $D_{\rm cm}$=17.0; 18.2; 19.3; 20.5; 21.6; and 22.7 fm and all eigenvalues (note that these $D_{\rm cm}$ values correspond to distances between the extremities of the nuclear shape which are, respectively: 28; 30; 32; 34; 36 and 38 fm).
- Second, for each $D_{\rm cm}$ value, we have fitted $P_{\rm TR}$ with the following function:

$$P_{\rm TR} = \frac{A-1}{1+\exp\left(\frac{Q_\alpha^{\rm SC}-Q_0}{a_Q}\right)} + 1, \qquad \text{(B.1)}$$

where A, Q_0 and a_Q are three free parameters. The calculated $P_{\rm TR}$ and the associated fits are shown in fig. 8.

- Third, we have searched a relation between these three parameters and $D_{\rm cm}$; we found (see fig. 9):

$$\begin{aligned} A &= -0.28 + 0.02 D_{\rm cm}, \\ Q_0 &= -40.16 + 6.35 D_{\rm cm} - 0.19\,(D_{\rm cm})^2, \\ a_Q &= 5.46 \times 10^{-9}\,(D_{\rm cm})^{6.616}. \end{aligned} \qquad \text{(B.2)}$$

Note that these relations are valid from $D_{\rm cm} \simeq$16 fm up to $D_{\rm cm} \simeq$23 fm. Combining eqs. (B.1) and (B.2) allows the calculation of $P_{\rm TR}$ for any $D_{\rm cm}$ and $Q_\alpha^{\rm SC}$ value.

References

1. O. Serot and C. Wagemans, Nucl. Phys. A **641** 34, (1998).
2. N. Carjan, J. Phys. **37** 1279, (1976); N. Carjan, Ph.D. Thesis, TH Darmstadt, 1977.
3. N. Carjan, A. Sandulescu and V.V. Pashkevich, Phys. Rev. C **11** 782, (1975).
4. I. Halpern, Ann. Rev. Nucl. Sci. **21** 245, (1971).
5. H. Schultheis and R. Schultheis, Phys. Rev. C **18** 1317, (1978).
6. U. Brosa, S. Grossman and A. Müller, Phys. Rep. **197** 167-262, (1990).
7. M. Brack, J. Damgaard, H.C. Pauli, A.S. Jensen, V.M. Strutinsky and C.Y. Wong, Rev. Mod. Phys. **44** 320, (1972).
8. A.R. Barett and J.S. Lilley, Phys. Rev. C **9** 2010, (1974).
9. R. Schäfer and T. Fliessbach, J. Phys. G **21** 861, (1995).
10. N. Carjan and B. Leroux, Phys. Rev. C **22** 2008, (1980).
11. N. Carjan, B. Leroux and J.P. Theobald, *Journées d'Etudes sur la Fission, Alpe d'Huez, IKDA 80/16 (1980)*; O. Serot, CENBG Rapport de DEA, 1987 (unpublished).
12. P. Heeg, Ph.D. thesis, TH Darmstadt, 1989.
13. J.P. Theobald, P. Heeg and M. Mutterer, Nucl. Phys. A **502** 343c, (1989).
14. O. Tanimura and T. Fliessbach, Z. Phys. A **328** 475, (1987).
15. V.A. Rubchenya and S.G. Yavshits, Z. Phys. A **329** 329, (1988).
16. V.A. Rubchenya, A.S. Roschin and S.G. Yavshits, *Workshop on Nuclear Fission and fission product spectroscopy*, ILL Grenoble, 1994, edited by H.Faust (Report FA05T, 199) p.26.
17. L. Demattè, C. Wagemans, R. Barthélémy, P. D'hondt and A. Deruytter, Nucl. Phys. A **617** 331-346, (1997).
18. J.P. Lestone, Phys. Rev. Lett. **70** 2245, (1993).
19. R.B. Firestone, *Table of Isotopes*, edited by V.S. Shirley, 8th edition vol. **2** (Wiley, New York, 1996).